

High-dimensional stochastic finite volumes using the tensor train format

Juliette Dubois¹ ^{*}, Michael Herty², Siegfried Müller²

06.02.2025

Abstract. A method for the uncertainty quantification of nonlinear hyperbolic equations with many uncertain parameters is presented. The method combines the stochastic finite volume method and tensor trains in a novel way: the physical space and time dimensions are kept as full tensors, while all stochastic dimensions are compressed together into a tensor train. The resulting hybrid format has one tensor train for each spatial cell and each time step. The MUSCL scheme is adapted to this hybrid format and the feasibility of the approach using several classical test cases is shown. For the Burgers' equation a convergence study and a comparison with the full tensor train format are done with three stochastic parameters. The equation is then solved for an increasing number of stochastic dimensions. The Euler equations are then considered. A parameter study and a comparison with the full tensor train format are performed with the Sod problem. For a complex application we consider the Shu-Osher problem. The presented method opens new avenues for combining uncertainty quantification with well-known numerical schemes for conservation laws.

Keywords. hyperbolic systems, stochastic finite volume method, tensor trains, low-rank approximation

MSCcodes. 65M08, 65M75, 35R60

1 Introduction

This work focuses on uncertainty quantification for nonlinear hyperbolic equations with many parameters. Various methods have been developed to study how uncertainties affect partial differential equations. Two main categories are Monte Carlo-type methods and the use of an orthogonal basis, for example with the generalized polynomial chaos expansion (gPC). The gPC method can be either intrusive, with e.g. stochastic Galerkin methods, or non-intrusive, e.g. stochastic collocation. The Monte Carlo method is non-intrusive and its convergence rate is independent of the problem dimension, but it converges very slowly. The gPC method has an exponential convergence rate when the solution of the equation depends smoothly on the stochastic parameters. This makes it well-suited for elliptic and parabolic equations, but the smooth dependency is in general not observed for hyperbolic problems.

Barth [1] introduced the stochastic finite volume method (SFV) to study hyperbolic equations with uncertainties. The SFV is a deterministic formulation of the equations that keeps some properties of the original hyperbolic problem, such as well-posedness [2]. However, since a new dimension is added for each uncertain parameter, solving numerically the equations quickly becomes impossible.

When adapting methods that were developed for low dimensions to high dimensions, the number of parameters at hand increases exponentially. This phenomenon is called the curse of dimensionality. Low-rank tensor formats appear as a possible solution to keep the storage and operations manageable. Low-rank tensors can be

¹Institut für Mathematik, Technische Universität Berlin, Straße des 17. Juni 136, 10623 Berlin, Germany

^{*}Corresponding author: dubois@math.tu-berlin.de

²Institut für Geometrie und Praktische Mathematik, RWTH Aachen University, Templergraben 55, D-52056 Aachen

seen as a generalization to tensors of the well-known low-rank matrix decomposition. Several tensor formats have been developed, among them the canonical, the Tucker and the hierarchical formats [3]. Here, we focus on one hierarchical format, namely the tensor train format. Tensor trains have been successfully used for solving elliptic, parabolic and linear hyperbolic problems [4–6]. The nonlinear hyperbolic case presents new difficulties because the structure is much less preserved over space and time: for example, shocks can appear. In [7], the authors propose to combine SFV with tensor trains and obtain promising results.

In this paper, we propose a hybrid formulation where — in contrast to [7] — the time and physical space are kept in the full format while the stochastic space is compressed in the tensor train format. Section 2 introduces the problem and presents the principle of the stochastic finite volume method. In Section 3 we recall the main ideas of the tensor train format. The new hybrid format is presented in Section 4. A MUSCL-type algorithm adapted to the hybrid format is then described. It highlights the few modifications needed to use tensor trains compared to the classical scheme. In Section 5, we show numerical experiments that prove the feasibility and efficiency of our approach.

2 The stochastic finite volume method

We are interested in conservation laws with uncertain initial data. The problem is presented in the one-dimensional space, but the method is the same for higher dimensions. Let $T > 0$, $\Omega_x \subset \mathbb{R}$, $\Omega_\xi \subset \mathbb{R}^m$, and let $\mathbf{u} : (0, T) \times \Omega_x \times \Omega_\xi \rightarrow \mathbb{R}^p$ be the solution to

$$\frac{\partial \mathbf{u}}{\partial t}(t, x; \omega_\xi) + \frac{\partial \mathbf{f}}{\partial x}(\mathbf{u}(t, x; \omega_\xi)) = \mathbf{0}, \quad x \in \Omega_x, \omega_\xi \in \Omega_\xi, t \in (0, T), \quad (1)$$

$$\mathbf{u}(0, x; \omega_\xi) = \mathbf{u}_0(x; \omega_\xi), \quad x \in \Omega_x, \omega_\xi \in \Omega_\xi. \quad (2)$$

Here, $\mathbf{f} = (f_1, \dots, f_p)$ is the flux field. The random input ω_ξ is parametrized by a random variable $\xi : \Omega \rightarrow \Omega_\xi$ defined on the probability space $(\Omega, \mathcal{F}, \mathbb{P})$. We assume that there exists a probability density $p : \mathbb{R}^m \rightarrow [0, \infty)$ such that the expectation and the variance for \mathbf{u} can be expressed as

$$\mathbb{E}[\mathbf{u}(t, x)] = \int_{\Omega_\xi} \mathbf{u}(t, x; \omega_\xi) p(\xi) d\xi, \quad \text{Var}[\mathbf{u}(t, x)] = \mathbb{E}[(\mathbf{u}(t, x) - \mathbb{E}[\mathbf{u}(t, x)])^2]. \quad (3)$$

2.1 General description of the method

The idea is to consider the space $\Omega_\xi \subset \mathbb{R}^m$ as new "spatial directions" of the problem [8]. The stochastic problem (1)-(2) is reformulated as a deterministic problem for the unknown $\mathbf{u}(t, x, \xi)$.

The physical space Ω_x and the parametrized probability space Ω_ξ are discretized as Cartesian grids, respectively denoted by \mathcal{C}_x and \mathcal{C}_ξ . The time interval $[0, T]$ is discretized with a time step Δt ,

$$\mathcal{C}_x = \cup_i K_x^i, \quad \mathcal{C}_\xi = \cup_j K_\xi^j, \quad [0, t] = \cup_k [t_k, t_k + \Delta t],$$

where $\mathbf{j} = (j_1, \dots, j_m)$ is a multi-index. We introduce a constant mesh size in the spatial direction Δx , and in each stochastic dimension $\Delta \xi_1, \dots, \Delta \xi_m$. The cells K_x^i and K_ξ^j are defined as

$$K_x^i = [x_{i-1/2}, x_{i+1/2}], \quad x_{i\pm 1/2} = x_i \pm \frac{\Delta x}{2}, \quad (4)$$

$$K_\xi^j = \prod_{\ell=1}^m [\xi_{j_\ell-1/2}, \xi_{j_\ell+1/2}], \quad \xi_{j_\ell\pm 1/2} = \xi_{j_\ell} \pm \frac{\Delta \xi_\ell}{2}. \quad (5)$$

Let N_x and $N_{\xi_1}, \dots, N_{\xi_m}$ denote the number of 1D cells in each spatial and stochastic direction, respectively.

We introduce the cell average in space

$$\mathbf{u}_i^n(\xi) = \frac{1}{|K_x^i|} \int_{K_x^i} \mathbf{u}(t^n, x, \xi) dx, \quad (6)$$

and the cell average in space and in expectation over a cell j

$$\bar{\mathbf{u}}_{i,j}^n = \frac{1}{|K_\xi^j|} \mathbb{E}_j[\mathbf{u}_{i,j}^n] = \frac{1}{|K_x^i| |K_\xi^j|} \int_{K_\xi^j} \int_{K_x^i} \mathbf{u}(t^n, x, \xi) dx p(\xi) d\xi. \quad (7)$$

Here the cell volumes are

$$|K_x^i| = \int_{K_x^i} dx = \Delta x, \quad |K_\xi^j| = \int_{K_\xi^j} p(\xi) d\xi. \quad (8)$$

Integrating Equation (1) in space and taking the expectation over a cell yields

$$\int_{K_\xi^j} \int_{K_x^i} \frac{\partial \mathbf{u}}{\partial t}(t^n, x, \xi) dx p(\xi) d\xi + \int_{K_\xi^j} \int_{K_x^i} \frac{\partial \mathbf{f}}{\partial x}(\mathbf{u}(t^n, x, \xi)) dx p(\xi) d\xi = \mathbf{0}. \quad (9)$$

After integration by parts, Equation (9) reads

$$\Delta x |K_\xi^j| \frac{d\bar{\mathbf{u}}_{i,j}^n}{dt} + \mathbb{E}_j[\mathbf{f}(\mathbf{u}(t, x_{i+1/2}, \xi)) - \mathbf{f}(\mathbf{u}(t, x_{i-1/2}, \xi))] = \mathbf{0}. \quad (10)$$

The exact flux \mathbf{f} is replaced by a numerical flux \mathcal{F} : the value of the solution at the interface $x_{i+1/2}$ is approximated using the values of the averages in the surrounding cells $\bar{\mathbf{u}}_{i-1,j}^n, \bar{\mathbf{u}}_{i,j}^n, \bar{\mathbf{u}}_{i+1,j}^n$. Let $\mathcal{F}_{i,j}^{n+}$ and $\mathcal{F}_{i,j}^{n-}$ denote the numerical flux at the interface $x_{i+1/2}$ and $x_{i-1/2}$, respectively. The approximation for their expectation over each cell is denoted by $\bar{\mathcal{F}}_{i,j}^{n+}$ and $\bar{\mathcal{F}}_{i,j}^{n-}$. Then Equation (10) is approximated by

$$\Delta x |K_\xi^j| \frac{d\bar{\mathbf{u}}_{i,j}^n}{dt} + \bar{\mathcal{F}}_{i,j}^{n+} - \bar{\mathcal{F}}_{i,j}^{n-} = 0, \quad \bar{\mathcal{F}}_{i,j}^{n+} = \mathbb{E}_j[\mathcal{F}^+(\mathbf{u}_{i,j}^n)], \quad \bar{\mathcal{F}}_{i,j}^{n-} = \mathbb{E}_j[\mathcal{F}^-(\mathbf{u}_{i,j}^n)]. \quad (11)$$

The integrals are approximated using the midpoint rule. The approximated average over a spatial cell is then

$$\bar{\mathbf{u}}_{i,j}^n \approx \mathbf{u}(t^n, x_i, \xi_j) \quad (12)$$

By abuse of notation, let $\bar{\mathbf{u}}_{i,j}^n$ and $\bar{\mathcal{F}}_{i,j}^{n\pm}$ denote respectively the expectation of the solution and the numerical fluxes, both computed with quadrature. The midpoint rule is used to compute the expectation \mathbb{E} with respect to p and, therefore, quantities are evaluated at the point ξ_j . We introduce the approximated volume for the stochastic cells $K_j = \Delta \xi_1 \dots \Delta \xi_m p(\xi_j)$. The semi-discrete equation reads then

$$K_j \Delta x \frac{d\bar{\mathbf{u}}_{i,j}^n}{dt} + K_j \bar{\mathcal{F}}_{i,j}^{n+} - K_j \bar{\mathcal{F}}_{i,j}^{n-} = \mathbf{0}. \quad (13)$$

After simplifications ($K_j \neq 0$), the semi-discrete scheme reads

$$\frac{d\bar{\mathbf{u}}_{i,j}^n}{dt} + \frac{1}{\Delta x} (\bar{\mathcal{F}}_{i,j}^{n+} - \bar{\mathcal{F}}_{i,j}^{n-}) = \mathbf{0}. \quad (14)$$

2.2 Numerical flux

The numerical flux is computed for a MUSCL scheme [9]. The expectation of the numerical flux at the interface $i+1/2$ is defined by

$$\bar{\mathbf{H}}_{i+1/2,j}^n = \frac{\mathbf{f}(\mathbf{u}_{i+1/2,j}^{n+}) + \mathbf{f}(\mathbf{u}_{i+1/2,j}^{n-})}{2} - \frac{a_{i+1/2,j}^n}{2} (\mathbf{u}_{i+1/2,j}^{n+} - \mathbf{u}_{i+1/2,j}^{n-}), \quad (15)$$

where intermediate values $\mathbf{u}_{i+1/2,j}^{n+}, \mathbf{u}_{i+1/2,j}^{n-}$ are linear reconstructions of the solution using the approximate derivative, and $a_{i+1/2,j}^n$ is the local speed.

The intermediate values are computed at the interface between two cells in space:

$$\mathbf{u}_{i+1/2,j}^{n+} = \bar{\mathbf{u}}_{i+1,j}^n - \frac{\Delta x}{2} (\mathbf{u}_x)_{i+1,j}^n \quad (16)$$

$$\mathbf{u}_{i+1/2,j}^{n-} = \bar{\mathbf{u}}_{i,j}^n + \frac{\Delta x}{2} (\mathbf{u}_x)_{i,j}^n \quad (17)$$

The approximation of the derivative $(\mathbf{u}_x)_{i,j}^n$ is obtained using a classical minmod limiter,

$$(\mathbf{u}_x)_{i,j}^n = \text{minmod} \left(\frac{\bar{\mathbf{u}}_{i,j}^n - \bar{\mathbf{u}}_{i-1,j}^n}{\Delta x}, \frac{\bar{\mathbf{u}}_{i+1,j}^n - \bar{\mathbf{u}}_{i,j}^n}{\Delta x} \right). \quad (18)$$

The local speed is given by

$$a_{i+1/2,j}^n = \max \left\{ \rho(\mathbf{f}'(\mathbf{u}_{i+1/2,j}^{n+})), \rho(\mathbf{f}'(\mathbf{u}_{i+1/2,j}^{n-})) \right\}, \quad (19)$$

where $\rho(\mathbf{A})$ denotes the spectral radius of the matrix \mathbf{A} . We recall that, if $\lambda_i(\mathbf{A})$ are the eigenvalues of \mathbf{A} , the spectral radius is defined by $\rho(\mathbf{A}) = \max_i |\lambda_i(\mathbf{A})|$.

2.3 Fully-discrete formulation and computational cost

We conclude the presentation of the stochastic finite volume method with the time discretization. A simple forward Euler scheme yields

$$\bar{\mathbf{u}}_{i,j}^{n+1} = \bar{\mathbf{u}}_{i,j}^n - \frac{\Delta t}{\Delta x} (\bar{\mathbf{H}}_{i+1/2,j}^n - \bar{\mathbf{H}}_{i-1/2,j}^n). \quad (20)$$

Note that in the case of a forward Euler discretization in time, the cell average in space is computed only for the initial condition. The cell average of the next time steps is directly given by (20).

Theoretically, the stochastic finite volume method has the advantage to give a complete description of the solution dependency to the random variables. However, the problem becomes computationally intractable when the dimension of the stochastic space Ω_ξ increases. Indeed, in the general case $m \geq 1$ with $N_{\xi_1}, \dots, N_{\xi_m}$ stochastic cells and N_t time steps, the discrete solution $\bar{\mathbf{u}}_{i,j}^n$ is a tensor with a number of entries growing exponentially with the number of directions:

$$(\bar{\mathbf{u}}_{i,j}^n)_{\substack{n=1, \dots, N_t \\ i=1, \dots, N_x \\ j=(1, \dots, 1), \dots, (N_{\xi_1}, \dots, N_{\xi_m})}} \in \mathbb{R}^{pN_t} \times \mathbb{R}^{pN_{\xi_1}} \times \dots \times \mathbb{R}^{pN_{\xi_d}} \times \mathbb{R}^{pN_{\xi_1}} \times \dots \times \mathbb{R}^{pN_{\xi_m}}. \quad (21)$$

For the considered problem, m can become very large, making the tensor $\bar{\mathbf{u}}_{i,j}^n$ too large for computation or storage. To circumvent this problem, we propose to use a low-rank tensor approximation. Following [7] we choose to use the tensor train format. Tensor trains are briefly described in the next section.

3 The tensor train format

Various low-rank formats for tensors have been proposed [3]. We focus on the tensor train format, which was introduced by [4] for numerical analysis.

3.1 Definition of a tensor train

For $m \in \mathbb{N}$, a m th-order tensor $T \in \mathbb{R}^{N_1 \times \dots \times N_m}$ is a tensor train if it can be written as a sum of products of third-order tensors,

$$T(i_1, \dots, i_m) = \sum_{\alpha_1, \dots, \alpha_m=1}^{r_1, \dots, r_m} G_1(i_1, \alpha_1) G_2(\alpha_1, i_2, \alpha_2) \cdots G_m(\alpha_m, i_m). \quad (22)$$

The third-order tensors $G_\ell \in \mathbb{R}^{r_{\ell-1} \times N_\ell \times r_\ell}$ are called the cores of the tensor train, and the values r_1, \dots, r_m are called the ranks. For the first and the last cores, the ranks are set to $r_0 = r_{m+1} = 1$. The tensor train rank (TT-rank) is the largest rank of the tensor train. We denote it by $r = \max_{\ell=1 \dots m} (r_\ell)$.

The tensor train format has two properties that make it well suited for our objective: it breaks the curse of dimensionality, and the associated approximation problem can be solved. Breaking the curse of dimensionality is a common goal of low-rank formats. For an m th-order tensor with N entries in each dimension, a total of N^m entries is required to describe the tensor. Adding new dimensions to the tensor increases exponentially the number of entries. For a tensor train, only $\mathcal{O}((m-2)Nr^2 + 2Nr)$ entries are necessary: adding new dimensions to a tensor train increases only polynomially its number of entries. Not all tensors have a low-rank representation, hence, for practical applications it is necessary to have some way of approximating a given tensor by a tensor in the low-rank format of choice. In this regard, the tensor train format is more convenient than other low-rank formats, the canonical decomposition for example. It was proved in [4] that the problem of finding a quasi-optimal tensor train approximation of a tensor for a given rank is well-posed. The proof is constructive, and the paper provides an algorithm to construct the quasi-optimal approximation. In contrast, the canonical decomposition has a higher compression rate, but its approximation problem is ill-posed [10].

3.2 Operations on tensor trains

Tensor trains allow for a range of algorithms for many common tensor operations. We list here the ones that will be used in the rest of the paper. Algebraic operations on tensors such as addition, element-wise multiplication, and tensor contraction can be done directly in the tensor train format by applying the appropriate operations on the cores. However, the resulting tensors have generally larger ranks. A rounding algorithm was introduced in [4]. The rounding of a tensor train consists in approximating it with a tensor train of a lower rank. This operation is again done directly in the tensor train format, and requires $\mathcal{O}(mNr^2 + mr^4)$ operations. Hence, after each algebraic operation, the result should be rounded to keep the rank low.

Applying a non-algebraic function to a tensor train is also possible thanks to the cross approximation algorithm. The cross approximation was first introduced in [11], and a version with adaptive ranks was developed in [12]. Cross approximation consists in evaluating the function at some entries of the tensor. Error estimates for the cross approximation algorithm have been developed in [13, 14] for element wise errors and in [15] for errors in the Frobenius norm. The main results of those papers is that the approximation error does not grow exponentially with the number of dimensions.

4 A hybrid format for the stochastic finite volume method

We propose here a method to solve hyperbolic equations with a high number of uncertain parameters. Our method takes advantage of the low-rank approximation while keeping the structure of deterministic solvers. The idea is to use the tensor train format only for the stochastic space, and to keep the full format in space and in time. We choose to keep a full format in time because we do not expect the solution to have a low-rank approximation with respect to time. The solution of a nonlinear hyperbolic problem can indeed significantly differ from the initial condition as time passes due to the steepening of gradients and, thus, discontinuities may develop. A comparison between low-rank approximation and full format in time was done in [6] for linear and quasi-linear hyperbolic problems. The authors observed that the full format in time was more accurate than its low-rank approximation, and we can expect the effect to be even more noticeable for nonlinear problems. Moreover, keeping the full format in space and in time allows us to adapt more easily well-known deterministic solvers. Most steps are indeed the same as a classical algorithm. The operations on scalars are simply replaced by operations on tensor trains, as we will describe in more detail later.

The low-rank format is used in the stochastic directions, where the number of dimensions is the largest. There is no theoretical argument ensuring that a problem starting with a low-rank structure keeps a low-rank structure. In previous works [16, 17], discontinuities were even observed in the stochastic direction, although there is no flux in this direction. However, previous results [7] give experimental evidence that low-rank formats can well approximate the solution. The method introduced in [7] consists in compressing physical and stochastic

spaces in a single tensor train. This single tensor train will be referred to as the "full-TT format" in the following.

Next, we discuss the proposed method in this manuscript. The method is stated for a scalar equation in a single spatial dimension and using the same discretization in each stochastic dimension. We define $\Delta\xi := \Delta\xi_1 = \Delta\xi_2 = \dots = \Delta\xi_m$, and $N_\xi := N_{\xi_1} = N_{\xi_2} = \dots = N_{\xi_m}$. A tensor train is used to approximate the solution for each spatial cell i , hence, the computational variable is an array of tensor trains:

$$\bar{U}^n = (\bar{U}_1^n, \dots, \bar{U}_{N_x}^n)^\top, \quad \text{with} \quad \bar{U}_i^n \approx (\bar{u}_{i,j}^n)_{j \in \{1, \dots, N_\xi\}^m}. \quad (23)$$

This hybrid-TT format is obtained by adding a new dimension to each core,

$$\bar{U}_i^n(j) = \sum_{\alpha_1, \dots, \alpha_m=1}^{r_1, \dots, r_m} G_1(i, j_1, \alpha_1) G_2(i, \alpha_1, j_2, \alpha_2) \cdots G_m(i, \alpha_m, j_m). \quad (24)$$

For comparison we state the full-TT format. Therein, a single tensor train with a core for the spatial variable is used:

$$\bar{U}^n(i, j) = \sum_{\alpha_1, \dots, \alpha_m=1}^{r_1, \dots, r_m} G_0(i, \alpha_0) G_1(\alpha_0, j_1, \alpha_1) G_2(\alpha_1, j_2, \alpha_2) \cdots G_m(\alpha_m, j_m). \quad (25)$$

An example of the approach is presented for the MUSCL finite-volume scheme with a first-order explicit in time integration for the hybrid and full-TT scheme, respectively. However, the idea is general and may be applied to any finite-volume scheme. We also state the computation of the expectation of variance with respect to ρ of the solution computed by the hybrid and full-TT schemes, respectively.

4.1 The MUSCL scheme in the hybrid format

The scheme from Section 2 is adapted to the hybrid format. The reconstructed states and the expectation of the numerical flux in the hybrid format are respectively denoted by $U^{n\pm} = (U_{3/2}^{n\pm}, \dots, U_{N_x+1/2}^{n\pm})^\top$, and $\bar{H}^n = (\bar{H}_{1/2}^n, \dots, \bar{H}_{N_x+1/2}^n)^\top$. We assume that, for a fixed cell i and time step n , the tensor train approximations \bar{U}_i^n and $U_{i+1/2}^{n+}$, $U_{i+1/2}^{n-}$ are given. Then, the MUSCL scheme in hybrid format reads:

$$\bar{U}_i^{n+1} = \bar{U}_i^n - \frac{\Delta t}{\Delta x} (\bar{H}_{i+1/2}^n - \bar{H}_{i-1/2}^n), \quad (26)$$

$$H_{i+1/2}^n = \frac{f(U_{i+1/2}^{n+}) + f(U_{i+1/2}^{n-})}{2} - \frac{a_{i+1/2}}{2} (U_{i+1/2}^{n+} - U_{i+1/2}^{n-}), \quad (27)$$

$$a_{i+1/2}^n = \max(|f'(U_{i+1/2}^{n+})|, |f'(U_{i+1/2}^{n-})|), \quad (28)$$

$$U_{i+1/2}^{n+} = \bar{U}_{i+1}^n - \frac{\Delta x}{2} (U_x)_{i+1}^n, \quad (29)$$

$$U_{i+1/2}^{n-} = \bar{U}_i^n + \frac{\Delta x}{2} (U_x)_i^n, \quad (30)$$

$$(U_x)_i^n = \text{minmod} \left(\frac{\bar{U}_i^n - \bar{U}_{i-1}^n}{\Delta x}, \frac{\bar{U}_{i+1}^n - \bar{U}_i^n}{\Delta x} \right). \quad (31)$$

Equations (26)-(31) are similar to a classical MUSCL scheme with no stochastic variables. The only difference is that the objects \bar{U}_i^n , $U_{i+1/2}^{n\pm}$, $(U_x)_i^n$ and $\bar{H}_{i+1/2}^n$ are scalars in the classical case, and tensor trains in our hybrid formulation. Hence, all operations on these objects must be adapted to the tensor train format. As explained in Section 3, linear and polynomial functions can be applied directly to tensor trains, whereas the cross-interpolation algorithm must be used for non-polynomial functions. In our case, the operations $(T_1, T_2) \mapsto \text{minmod}(T_1, T_2)$ and the function $(T_1, T_2) \mapsto \max(|T_1|, |T_2|)$ are non-polynomial in the variables T_1, T_2 . Depending on the problem at hand, this can also be the case for the initial condition u_0 , the flux f and its derivative f' .

The first step of the algorithm is to compute the cell average of the initial condition in the hybrid format \bar{U}^0 using (12). The case for systems of equations will be described in Section 5.2. For scalar equations, we use the

maximum principle $|u(t, x, \xi)| \leq \max_{x, \xi} |u_0(x, \xi)|$ to set the fixed time step

$$\Delta t < \frac{1}{2} \frac{\Delta x}{\max |f'(\bar{U}^0)|}. \quad (32)$$

The solution is then propagated in time using the scheme (26)-(31). The algorithms are summarized in Appendix A.

4.2 Computing expectation and variance

Once the solution in the hybrid format \bar{U} is known, we compute its expectation and variance. For simplicity, we describe the computation for two stochastic variables $\xi = (\xi_1, \xi_2)$. The expectation and variance of the solution u at time t and point x are

$$\mathbb{E}[u(t, x)] = \int_{\Omega_\xi} u(t, x, \xi_1, \xi_2) p_{\xi_1, \xi_2}(\xi_1, \xi_2) d\xi_1 d\xi_2, \quad (33)$$

$$\text{Var}[u(t, x)] = \mathbb{E}[(u(t, x) - \mathbb{E}[u(t, x)])^2] = \mathbb{E}[u(t, x)^2] - \mathbb{E}[u(t, x)]^2. \quad (34)$$

We make the additional assumption that the random variables are independent and denote by p_1, p_2 the probability distributions associated to ξ_1 and ξ_2 , respectively. The integral over the whole space Ω_ξ is approximated as a sum

$$\mathbb{E}[u_i^n] \approx \sum_{j_1=1}^{N_\xi} \sum_{j_2=1}^{N_\xi} \bar{u}_{i, j_1, j_2}^n p_1(\xi_{j_1}) p_2(\xi_{j_2}) (\Delta \xi)^2. \quad (35)$$

This operation can be seen as a contraction of the tensor \bar{u}_{i, j_1, j_2}^n with the tensor $p(\xi_{j_1})p(\xi_{j_2})$. Moreover, the tensor $p(\xi_{j_1})p(\xi_{j_2})$ is a tensor train with rank 1 and cores $p(\xi_{j_1})$ and $p(\xi_{j_2})$. With the solution in the hybrid format \bar{U}_i^n , the tensor contraction can be computed in the tensor train format. For the variance, the squared solution is first computed in the hybrid format by operation on tensor trains, then its expectation is obtained as above. The variance is then computed using Equation (34).

4.3 The fully-TT format for the MUSCL scheme

We compare the proposed approach with the full-TT approach. For this, the method introduced in [7] is stated for the MUSCL scheme. The core idea is to rewrite the scheme (15)-(20) in terms of global matrices. Then, every computational operation is applied to the full TT approximation of the solution, using either TT algebraic operations or cross-approximation.

We illustrate the idea by describing the reconstruction step with global matrices. For simplicity, the operation is first described in the scalar case and a single spatial variable and without any stochastic variables. Let $\bar{u}^n = (u_1^n, \dots, u_{N_x}^n)$ be the solution vector. We introduce the identity matrix $\mathbf{I} \in \mathbb{R}^{N_x \times N_x}$ and the matrices $\mathbf{L}, \mathbf{R} \in \mathbb{R}^{N_x \times N_x}$ defined by

$$\mathbf{L} = \begin{pmatrix} 0 & 0 & 0 & \dots & 0 \\ 1 & 0 & 0 & \dots & 0 \\ 0 & 1 & 0 & \dots & 0 \\ \vdots & \vdots & \vdots & \vdots & \vdots \\ 0 & 0 & \dots & 0 & 0 \\ 0 & 0 & \dots & 1 & 0 \end{pmatrix} \text{ and } \mathbf{R} = \begin{pmatrix} 0 & 1 & 0 & \dots & 0 \\ 0 & 0 & 1 & \dots & 0 \\ 0 & 0 & 0 & \dots & 0 \\ \vdots & \vdots & \vdots & \vdots & \vdots \\ 0 & 0 & \dots & 0 & 1 \\ 0 & 0 & \dots & 0 & 0 \end{pmatrix}.$$

The vector of approximate derivatives defined in (18) is obtained as matrix vector multiplication with the defined matrices, i.e.,

$$(u_x)^n = \frac{1}{\Delta x} \text{minmod}((\mathbf{I} - \mathbf{L})\bar{u}^n, (\mathbf{R} - \mathbf{I})\bar{u}^n), \quad (36)$$

and the MUSCL scheme then computes the right and left states at the cell interfaces, denoted by $u^{n\pm} = (u_{3/2}^{n\pm}, \dots, u_{N_x+1/2}^{n\pm})$ and defined with (16),

$$u^{n\pm} = \bar{u}^n \pm \frac{\Delta x}{2} (u_x)^n. \quad (37)$$

In the case of m stochastic variables, the solution is approximated as a tensor train using the representation (25). Now, the previous computations are repeated on the tensor train format. Since the operation of shifting an index to the right or to the left (given by the previously defined matrices) is only applied to the spatial indices, only the spatial core G_0 of the representation is affected. For example, the right-shifted core \tilde{G}_0 is given by $\tilde{G}_0 = \mathbf{R}G_0$, and the tensor-train for the right-shifted solution is

$$\bar{U}^n(i+1, j) = \sum_{\alpha_1 \dots \alpha_m=1}^{r_1 \dots r_m} \tilde{G}_0(i, \alpha_1) G_1(\alpha_0, j_1, \alpha_1) G_2(\alpha_1, j_2, \alpha_2) \dots G_m(\alpha_m, j_m). \quad (38)$$

The approximate derivative in the TT format is thus obtained by computing the left- and right-shifted cores and by applying the minmod limiter to the resulting tensor trains. The later requires e.g. cross-approximation on the tensor train format. The full-TT approximation in the MUSCL scheme is then summarized in Algorithm 3. The remaining operations are linear on the tensor train and their description is omitted. Finally, expectation and variance are obtained by integration that is done by contracting the solution tensor with the rank-one tensor of integration weights.

5 Numerical results

In this section, we apply the method to three hyperbolic problems: the Riemann problem associated to Burgers' equation, the Sod problem and the Shu-Osher problem for the Euler equations. For the first problem, we investigate the influence of some parameters on the algorithm accuracy, and compare it to the full-TT format. We also show that the method can scale up for a larger number of stochastic dimensions. The second problem showcases the method's applicability to a system of equations. A parameter study and a comparison with the full-TT format are presented. Finally, the last test case shows the method's ability to handle a complex interaction problem.

The method was implemented in python with the tntorch library [18].

5.1 Stochastic Burgers' equation

We consider the Burgers' equation with uncertain initial conditions

$$\frac{\partial u}{\partial t} + \frac{1}{2} \frac{\partial u^2}{\partial x} = 0, \quad u_0(x, \xi) = \begin{cases} 1 + \sum_{\ell=1}^m v_{L,\ell} \xi_\ell, & x < 0 \\ -1 + \sum_{\ell=1}^m v_{R,\ell} \xi_\ell, & x > 0 \end{cases}. \quad (39)$$

The random variables are assumed independent with $\xi_\ell \sim \mathcal{U}(0, 1)$, for all $\ell \in \{1, \dots, m\}$. Computations are performed for $\Omega_x = (-1, 1)$ until final time $T = 0.35$, and we use the CFL number $\alpha = 0.45$. Let $\mathbf{v}_L = (v_{L,1}, \dots, v_{L,m})^\top$ and $\mathbf{v}_R = (v_{R,1}, \dots, v_{R,m})^\top$. For now, the number m of random variables is arbitrary. The value of m and of the coefficients $\mathbf{v}_L, \mathbf{v}_R$ will be given in each subsection. We focus on the case where the solution is a shock wave, hence, we assume that for all realizations of $\xi = (\xi_1, \dots, \xi_m)$ it holds

$$1 + \sum_{\ell=1}^m v_{L,\ell} \xi_\ell > -1 + \sum_{\ell=1}^m v_{R,\ell} \xi_\ell. \quad (40)$$

Under this assumption, the exact solution to (39) is a shock

$$u(t, x, \xi) = \begin{cases} u_L(\xi), & x < s(\xi)t \\ u_R(\xi), & x > s(\xi)t \end{cases}, \quad s(\xi) = \frac{u_L(\xi) + u_R(\xi)}{2}. \quad (41)$$

In the following, we focus on the case $m = 3$ and study the algorithmic performance for an increasing number of (spatial and stochastic) cells. Then, we consider the scale-up possibility by increasing m .

5.1.1 Convergence study and influence of parameters

We choose $m = 3$ and take the following initial conditions

$$u_0(x, \xi) = \begin{cases} 1 + 0.1\xi_1 - 0.1\xi_3, & x < 0 \\ -1 + 0.1\xi_1 - 0.1\xi_2, & x > 0 \end{cases}. \quad (42)$$

We investigate the influence of some parameters on the performance of the algorithm.

The number of stochastic and spatial cells, the TT-rank, and the tolerance for TT approximations are varied, and the relative L^1 -error of the expectation, the relative L^1 -error of the variance, and the number of coefficients for the hybrid format at final time are computed. The relative L^1 -error for the expectation at final time T is defined by

$$|\mathbb{E}|_{L^1, \text{rel}} = \frac{|\mathbb{E}_{TT} - \mathbb{E}_{\text{ex}}|_{L^1}}{|\mathbb{E}_{\text{ex}}|_{L^1}}. \quad (43)$$

The exact expectation along x is approximated using the midpoint rule, and the relative error is computed with

$$|\mathbb{E}|_{L^1} = \frac{1}{N_x} \sum_{i=1}^{N_x} \mathbb{E}[\bar{u}_i^n], \quad |\mathbb{E}_{TT} - \mathbb{E}_{\text{ex}}|_{L^1} = \frac{1}{N_x} \sum_{i=1}^{N_x} \left(\mathbb{E}[U_i^n] - \int_{x_{i-1/2}}^{x_{i+1/2}} \mathbb{E}[u(x, t)] \right). \quad (44)$$

The relative L^1 -error for the variance $|\text{var}|_{L^1, \text{rel}}$ is defined similarly. The expectation for the tensor train $\mathbb{E}[U_i^n]$ is computed as described in Section 4.2. The expectation and the variance of the exact solution are given in Appendix B. Since their expression requires nontrivial integration, the integrals are numerically approximated using the `scipy.integrate` package [19].

The number of cells in the spatial direction is denoted by N_x . Each stochastic direction has the same discretization, and we denote by N_ξ the number of cells for each stochastic direction. For example, in the case $N_x = N_\xi = 160$, the spatial-stochastic grid is made of 160^4 cells. The TT-rank r_{\max} corresponds to the maximal rank allowed for each rounding operation. The tolerance ε is a parameter related to the cross approximation algorithm and the rounding operations. It should be noted that this tolerance does not give a global error on the tensor approximation, so its influence on the total error of the algorithm is not known. Table 5.1.1 shows the tested parameters. The maximal rank actually observed for each simulation is denoted by r in the table.

We first note that for the expectation, except for the case $\varepsilon = 0.1$, all combinations of ε and r_{\max} result in quite similar convergence curves. When $\varepsilon < 0.1$, the convergence order is close to one for the expectation and one half for the variance. Those orders are in agreement with the one-half order predicted by the theory [8]. For the case $\varepsilon = 0.1$, the TT approximation is not precise enough, and the expected convergence rate is not reached. This behavior was also observed in [7] for the full-TT discretization. The lowest rank $r_{\max} = 1$ seems to be as good as larger ranks for the expectation, but not for the variance. From Table 5.1.1, we see that the maximal rank r_{\max} is more often reached the larger N_x and the smaller ε . Finally, we note that during the simulations, warnings indicated that the cross-interpolation was not converging, even when r_{\max} is not reached and even though the final errors are reasonable.

The convergence study was also done by varying only N_x and fixing $N_\xi = 20$. Figure 2 shows the resulting convergence curves. They are very similar to the case $N_\xi = N_x$, indicating that the convergence rate is mostly driven by the accuracy in x .

We also compare the performance of the hybrid format to the full-TT format. Figure 3 shows the convergence curve of the hybrid and the full-TT format using the values of ε and r_{\max} given in Table 5.1.1. The case $\varepsilon = 0.1$ yields better results for the hybrid format than for the full-TT format. For smaller ε , both methods yield comparable results. In this case, the full-TT method is more efficient since it requires fewer tensor coefficients: for the same maximal rank r , the hybrid method requires N_ξ times more parameters. Figure 4 shows how the number of coefficients at final time increases with N_x for each method, compared to the theoretical number of parameter for the full discretization. We use $\varepsilon = 10^{-3}$, $r_{\max} = 5$ and $N_\xi = N_x$. As expected, the full-TT format has a lower number of coefficients than the hybrid format, and both methods provide a significant compression compared to the full tensor.

$\varepsilon = 10^{-1}$				$\varepsilon = 10^{-3}$				$\varepsilon = 10^{-5}$			
N_x	r_{\max}	r (h)	r (f)	N_x	r_{\max}	r (h)	r (f)	N_x	r_{\max}	r (h)	r (f)
20	1	1	1	20	1	1	1	20	1	1	1
	5	2	1		5	2	3		5	5	5
	10	2	1		10	2	3		10	8	10
	30	2	1		30	2	3		30	12	13
40	1	1	1	40	1	1	1	40	1	1	1
	5	2	1		5	5	4		5	5	5
	10	2	1		10	6	4		10	10	10
	30	2	1		30	8	5		30	30	30
80	1	1	1	80	1	1	1	80	1	1	1
	5	2	1		5	5	5		5	5	5
	10	2	1		10	9	6		10	10	10
	30	2	1		30	12	7		30	30	30
160	1	1	1	160	1	1	1	160	1	1	1
	5	2	1		5	5	5		5	5	5
	10	2	1		10	10	7		10	10	10
	30	2	1		30	15	7		30	30	30

Table 1: Parameters tested for Sections 5.1.1. The maximal rank observed for the hybrid and the full-TT format in the case $N_\xi = N_x$ are respectively denoted by r (h) and r (f).

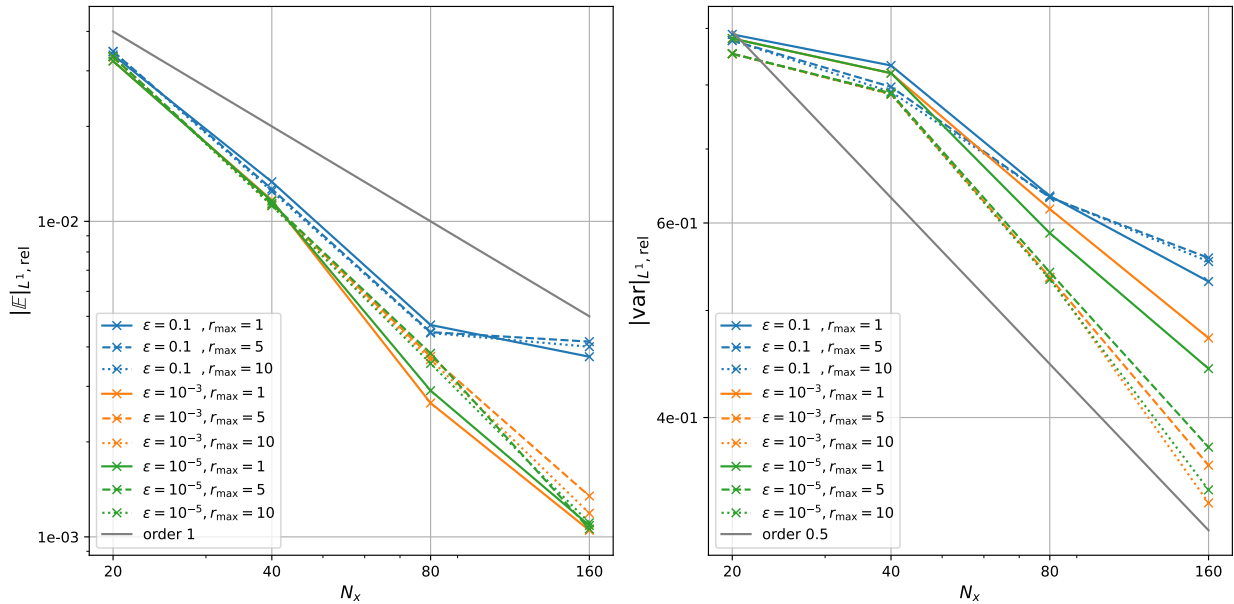


Figure 1: Relative L^1 -errors of the expectation and variance for the shock wave, computed with $N_\xi = N_x$ using the hybrid method.

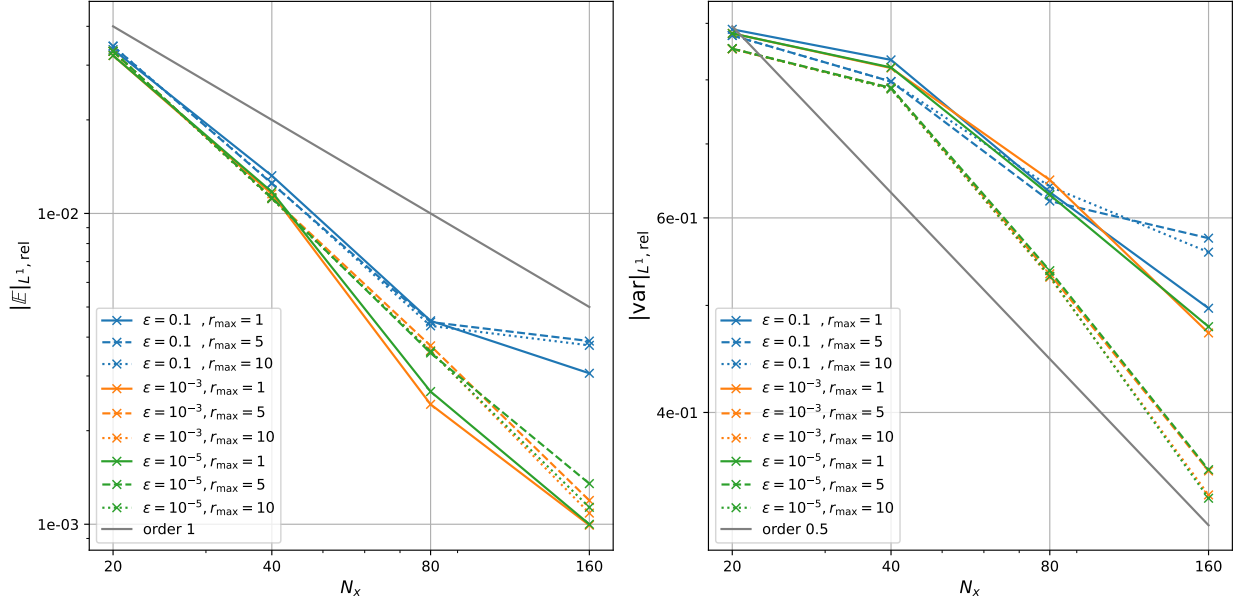


Figure 2: Relative L^1 -errors of the expectation and variance for the shock wave, computed with $N_\xi = 20$ using the hybrid method.

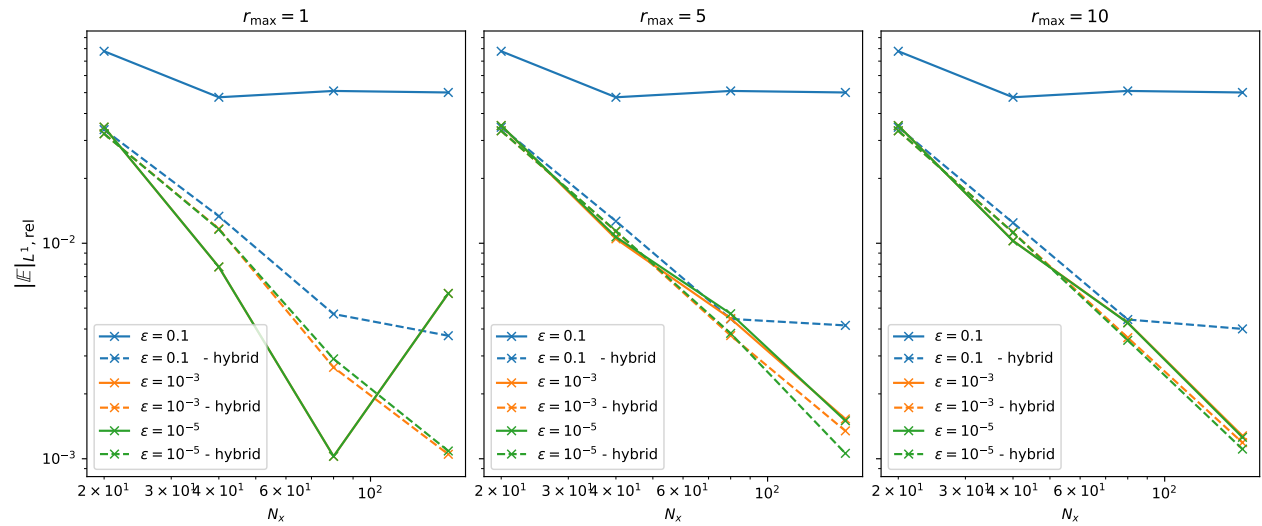


Figure 3: Relative L^1 -error of the expectation for the shock wave, using the full-TT (plain line) and hybrid (dashed line) formats.

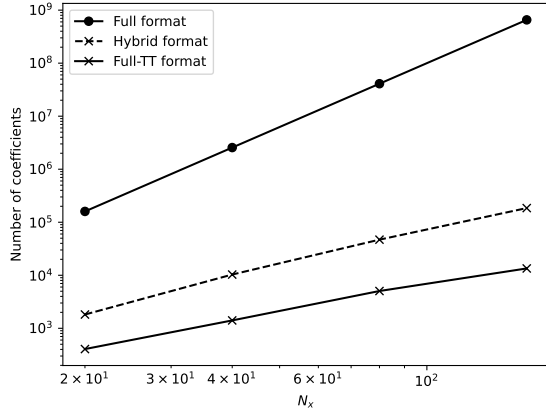


Figure 4: Number of coefficients of the solution at the final time: hybrid format, full-TT format, and theoretical value for the full tensor.

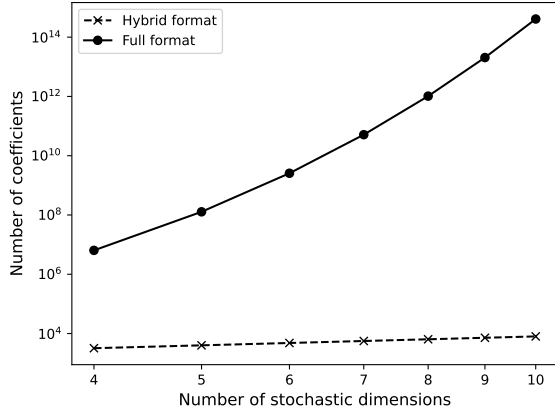


Figure 5: Number of coefficients of the solution at the final time for increasing stochastic dimensions: hybrid format and theoretical value for the full tensor

5.1.2 Scaling study

We now investigate the scalability of the method. We fix $N_x = 40$, $N_\xi = 20$, $r_{\max} = 5$, $\varepsilon = 0.01$ and vary the number of stochastic dimensions m . The coefficients $\mathbf{v}_R, \mathbf{v}_L$ are $v_{R,\ell} = 0.1$, $v_{L,\ell} = -0.1$ for $\ell \in \{1, \dots, m\}$. This ensures that the solution is a shock wave, no matter the number of stochastic dimensions. Thus, the expectation will exhibit a discontinuity at around $x = 0$, see Figure 6.

Figure 5 shows the number of entries for the solution at the final time and compare it with the number of entries for the full tensor. The number of entries for the hybrid format is polynomial with respect to the number of stochastic dimensions, whereas it is exponential for the full format. When running the experiment, we noticed that the cross approximation algorithm did not always converge. The cross approximation failed to converge more frequently with increasing dimensions. To check how much the convergence of the cross approximation alters the solution, we show in Figure 6 the expectation of the solution. The numerical solution seems not to be affected by the failed convergence: a shock is still visible at the expected location.

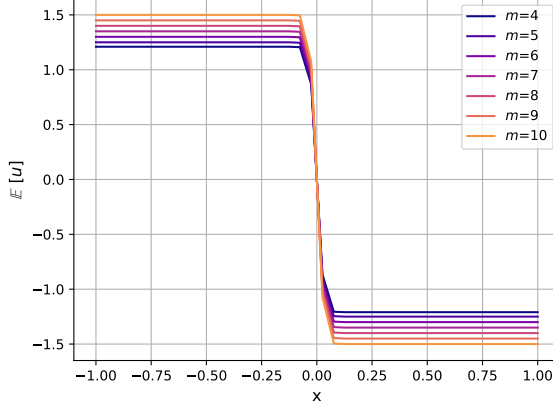


Figure 6: Expectation of the solution as a function of x , for various numbers of stochastic dimensions m .

5.2 Sod problem

The second experiment is the Sod problem for the Euler equations. We use this example to show that the algorithm can be extended to systems, and that the approximated solution can capture features such as shocks and contact waves typical for nonlinear hyperbolic problems. We also investigate the influence of the mesh size and the rank on the solution.

5.2.1 Problem description

We consider the Euler equations in one spatial dimension,

$$\frac{\partial}{\partial t} \begin{pmatrix} \rho \\ \rho u \\ \rho E \end{pmatrix} + \frac{\partial}{\partial x} \begin{pmatrix} \rho u \\ \rho u^2 + p \\ (\rho E + p)u \end{pmatrix} = 0. \quad (45)$$

Here ρ is the density, u the velocity, E the total energy, p the pressure. For a perfect gas with specific heat ratio $\gamma = 1.4$, the pressure is given by

$$p = (\gamma - 1) \left(\rho E - \frac{\rho u^2}{2} \right). \quad (46)$$

Note that compared to the Burgers' equation, the flux of the Euler equations consists of non-polynomial functions. Hence, cross approximation is required for the flux evaluation. We consider the Sod shock tube problem for $x \in (0, 1)$ with free boundary conditions and with $m = 3$ stochastic directions,

$$\begin{pmatrix} \rho(0, x, \xi) \\ u(0, x, \xi) \\ p(0, x, \xi) \end{pmatrix} = \begin{cases} \begin{pmatrix} 1 + 0.1\xi_1 + 0.1\xi_2 + 0.05\xi_3 \\ -0.01\xi_1 + 0.05\xi_2 + 0.01\xi_3 \\ 1 + 0.1\xi_1 - 0.01\xi_2 + 0.01\xi_3 \end{pmatrix}, & 0 < x < 0.5 \\ \begin{pmatrix} 0.125 + 0.05\xi_1 - 0.05\xi_2 + 0.01\xi_3 \\ 0.05\xi_1 - 0.01\xi_2 \\ 0.1 + 0.01\xi_1 + 0.05\xi_2 - 0.01\xi_3 \end{pmatrix}, & 0.5 < x < 1 \end{cases}. \quad (47)$$

The random variables are assumed independent and $\xi_\ell \sim \mathcal{U}(0, 1)$, for all $\ell \in \{1, \dots, m\}$. Here, the time step is updated at each iteration. For a hyperbolic system with eigenvalues $\lambda_1, \dots, \lambda_p$, the CFL condition has the form

$$\frac{\Delta t}{\Delta x} \max_p |\lambda_p| < \alpha, \quad (48)$$

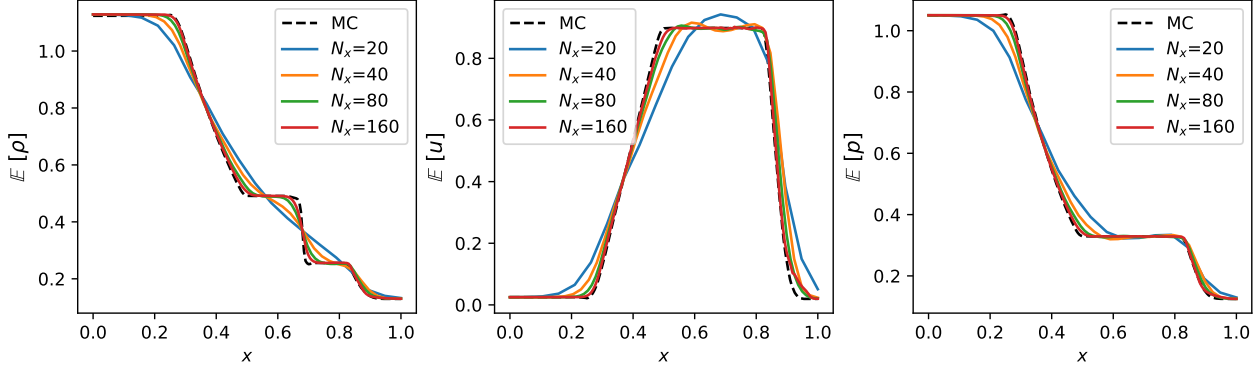


Figure 7: Expectation of ρ, u, p for $r_{\max} = 5, N_\xi = 20$ and $N_x \in \{20, 40, 80, 160\}$. The MC result (dashed line) is plotted for reference.

and we use the CFL number $\alpha = 0.4$. The eigenvalues of the Euler equations are

$$\lambda_1 = u - c, \quad \lambda_2 = u, \quad \lambda_3 = u + c, \quad c = \sqrt{\frac{\gamma p}{\rho}}. \quad (49)$$

5.2.2 Parameter study

We investigate the influence of N_x, N_ξ and r_{\max} on the solution. The tolerance for TT approximations, that was varied in the Burgers case, is fixed here at $\varepsilon = 0.01$. Since there is no analytical solution known for the stochastic Sod problem, we focus here on the qualitative results. We plot the expectation and variance of the primitive variables at final time $T = 0.2$. For comparison, the expectation and variance are also computed using a Monte-Carlo (MC) method with the library MultiWave [20]: an adaptive discontinuous Galerkin solver was used with $L = 6$ refinement levels corresponding to a uniformly refined grid with 192 cells and polynomial elements of degree 2, i.e., third-order scheme; the expectation and variance were computed with 125,000 samples. Details can be found in [16, 17, 21] where similar Monte-Carlo simulations were performed.

Figures 7 and 8 respectively show the expectation and variance of the primitive variable for $r = 5, N_\xi = 20$ and for various mesh refinement in the physical space N_x . For the expectation, there are little differences between $N_x = 80$ and $N_x = 160$ indicating convergence of the scheme. The general shape is globally in good agreement with the MC results. In transition between the contact wave and the shock wave at $x \in [0.65, 0.85]$, there are non-physical oscillations. These oscillations are also present in the deterministic Euler equations when solving with a MUSCL scheme and a leap-frog time-stepping. Hence, they are probably not related to the stochastic problem, and will not be further investigated in this work. The MC results are sharper, as they are obtained with a third-order DG solver.

To study the influence of the rank, we set $N_x = 160, N_\xi = 20$ and vary the maximal rank r_{\max} . The expectation and variance of ρ, u, p are shown in Figure 9 and in Figure 10 respectively. For r_{\max} larger than 5, the results are very similar. We also tested ranks lower than 5, but the solution became non-physical after some time. Figure 11 shows the actual maximal rank at final time in each spatial cell for the case $N_x = 160, N_\xi = 20$ and $r_{\max} = 10$. In most cells, the ranks are very low – less than three – and the large ranks concentrate in few cells around the shock. Hence, large ranks are needed only in localized regions. Moreover, they can provide information on the spatial structure of the solution.

Finally, we fix $N_x = 160, r = 5$ and vary N_ξ . Figure 12 shows the expectation of ρ, u, p . The number of stochastic cells does not seem to have a significant influence, which is probably due to the choice of a uniform probability distribution for each random variable. It should be noted that the case $N_\xi = 40$ yields non-physical solutions, hence it is not included here.

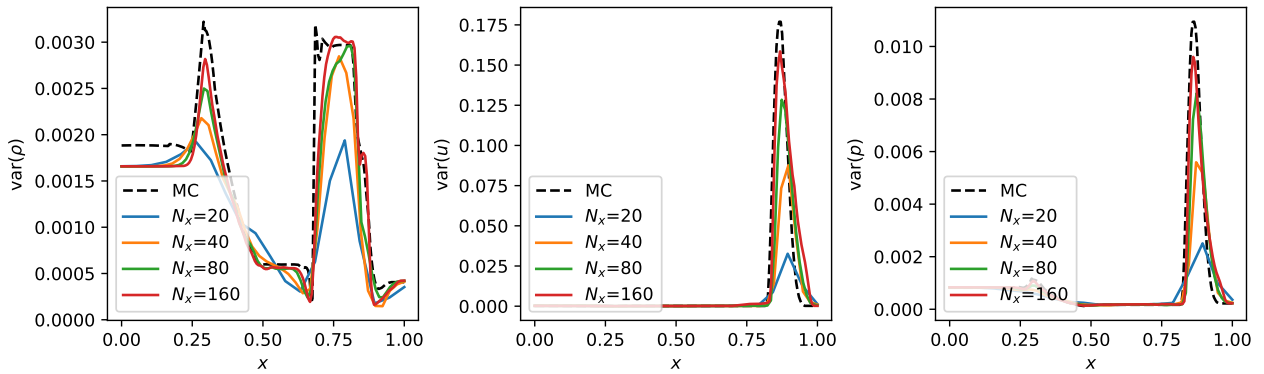


Figure 8: Variance of ρ, u, p for $r_{\max} = 5$, $N_\xi = 20$ and $N_x \in \{20, 40, 80, 160\}$. The MC result (dashed line) is plotted for reference

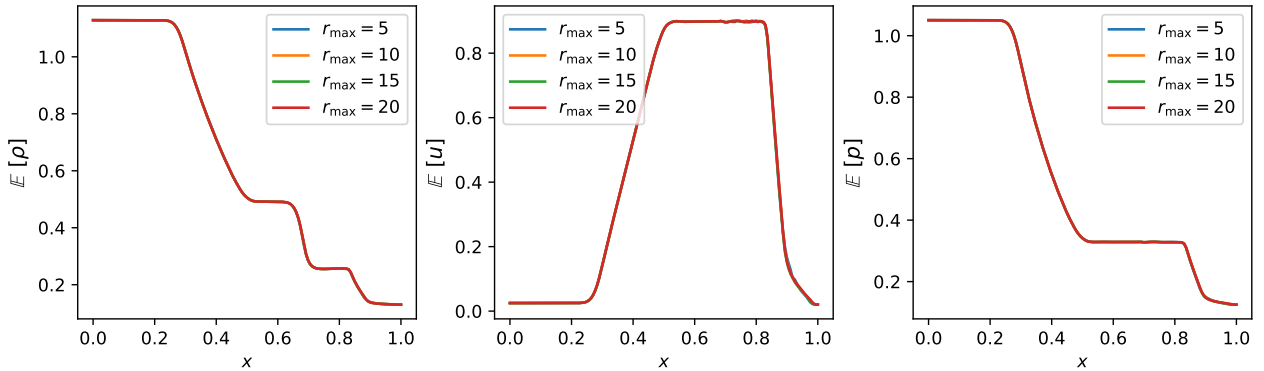


Figure 9: Expectation of ρ, u, p for $N_x = 160$, $N_\xi = 20$, and $r_{\max} \in \{5, 10, 15, 20\}$.

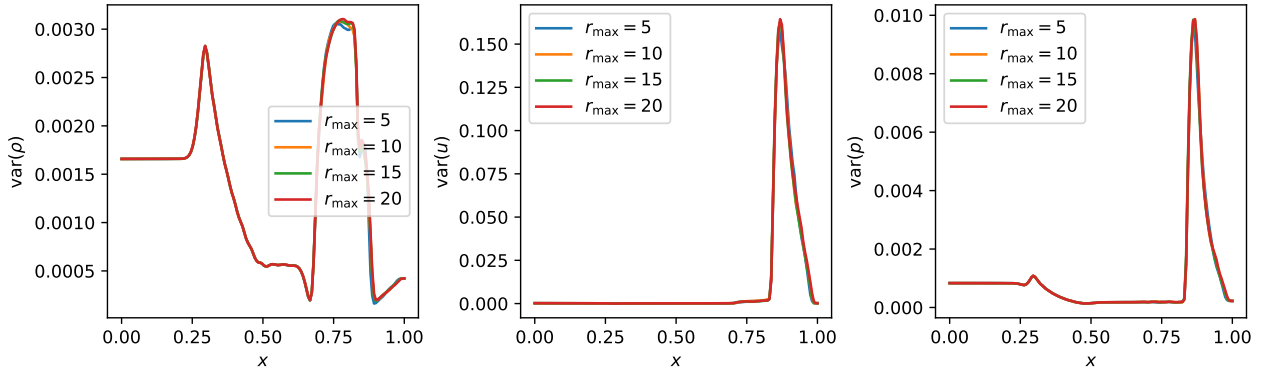


Figure 10: Variance of ρ, u, p for $N_x = 160$, $N_\xi = 20$, and $r_{\max} \in \{5, 10, 15, 20\}$.

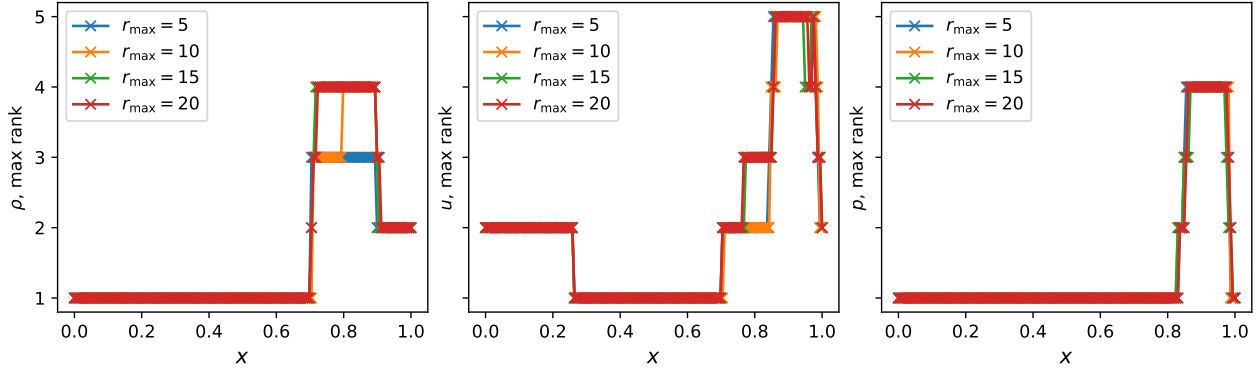


Figure 11: Maximal rank observed at final time for each spatial cell in the hybrid format of ρ, u, p for $N_x = 160, N_\xi = 20, r_{\max} \in \{5, 10, 15, 20\}$.

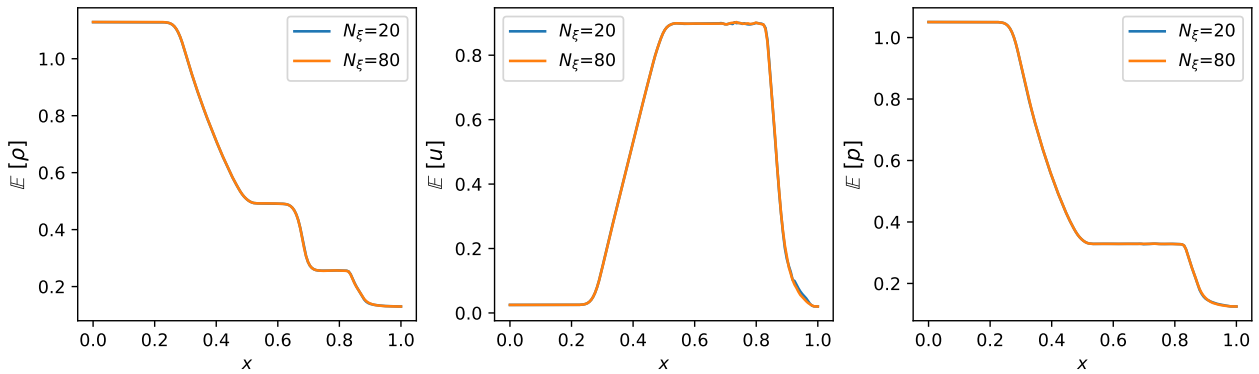


Figure 12: Expectation of ρ, u, p for $N_x = 160, r_{\max} = 5$ and $N_\xi \in \{20, 80\}$.

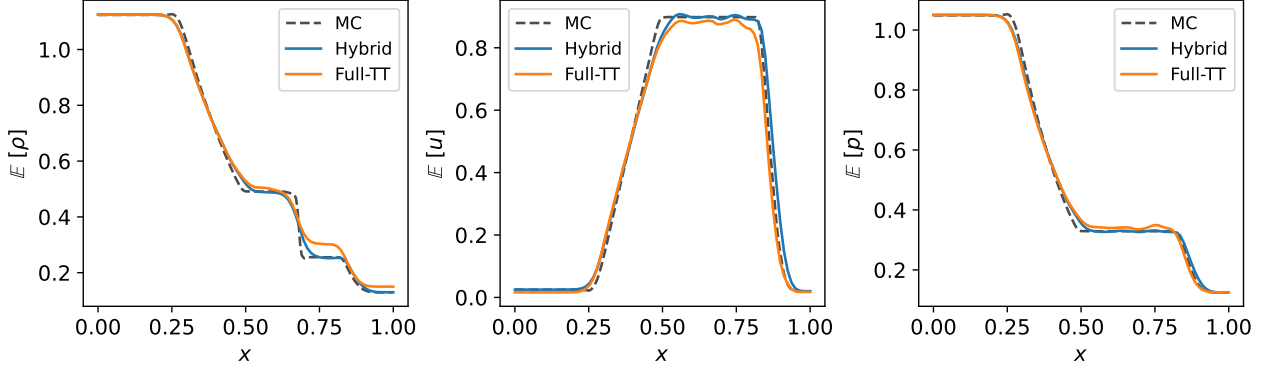


Figure 13: Expectation of ρ, u, p for the full-TT format and the hybrid format for $N_x = 80, N_\xi = 20$ and $r_{\max} = 10$. The MC result (dashed line) is plotted for reference.

5.2.3 Comparison with the full-TT format

The results obtained with the hybrid format are compared with the full-TT formats. Figure 13 shows the expectation of ρ, u, p using $N_x = 80, N_\xi = 20, \varepsilon = 10^{-3}, r_{\max} = 10$ for both formats. The MC result is used as reference. We see that the hybrid format is slightly more accurate than the full-TT format, in particular for the density and around the shock. However, with our current implementation, the hybrid format ran for much longer than the full-TT format: it took approximately two hours to complete, against ten minutes for the full-TT format. The number of coefficients at final time is also much larger for the hybrid format. Those two aspects could be greatly improved by improving the finite volume scheme, using e.g. a higher-order method and a non-uniform mesh in the space direction.

For the Sod problem, a low rank representation is sufficient in most places, but higher rank are necessary in some local parts. This example illustrates how we can use the hybrid format to gain more precise information on the problem.

5.3 Shu-Osher problem

The last experiment is the Shu-Osher problem for the Euler system (45)-(46). In this test case, a shock wave interacts with a sine wave density. The solution includes a shock wave and small-scale variations. Two stochastic variables are added in the initial data to extend the dimension. For $\xi_1 = \xi_2 = 0$, we recover the the classical definition of the problem. The initial condition for the random problem in primitive variables are given by

$$\begin{pmatrix} \rho(0, x, \xi), \\ u(0, x, \xi), \\ p(0, x, \xi) \end{pmatrix} = \begin{cases} \begin{pmatrix} 3.857143 + 0.1\xi_1 \\ 2.629369 + 0.1\xi_1 \\ 10.33333 + \xi_1 \end{pmatrix}, & 0 < x < \frac{1}{8} \\ \begin{pmatrix} 1 + 0.2(1 + \xi_2) \sin(16\pi x) \\ 0.0 \\ 1. + 0.1\xi_2 \end{pmatrix}, & \frac{1}{8} < x < 1 \end{cases}. \quad (50)$$

The simulation was run until time $t = 0.13$. The following parameters are used for the discretization: $N_x = 1600, N_\xi = 20, r_{\max} = 5, \varepsilon = 0.01$. We also run tests with a smaller maximal rank r_{\max} and a larger ε , but the solution in that case yields negative densities. Therefore, those results are omitted. The relatively high rank indicates that a strong compression of the solution is not necessarily expected for this problem.

Figure 14 shows the expectation and the standard deviation σ for ρ, u, p . We see that the standard deviation is large near the shock, in particular in the results for the density. Figure 15 shows the maximal ranks in each spatial cell at the final time for ρ, u, p . Interestingly enough, most cells have a very low rank: $r \leq 2$. The largest ranks are, as in the Sod case, concentrated near the shock. This is also expected due to the low regularity of

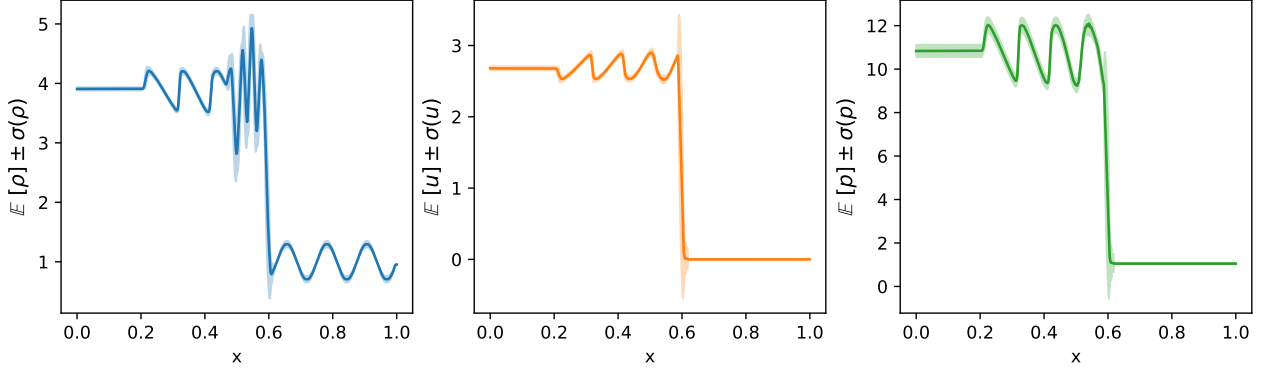


Figure 14: Expectation and standard deviation for ρ, u, p at final time. The results were obtained with $N_x = 1600, N_\xi = 20, r_{\max} = 5, \varepsilon = 0.01$.

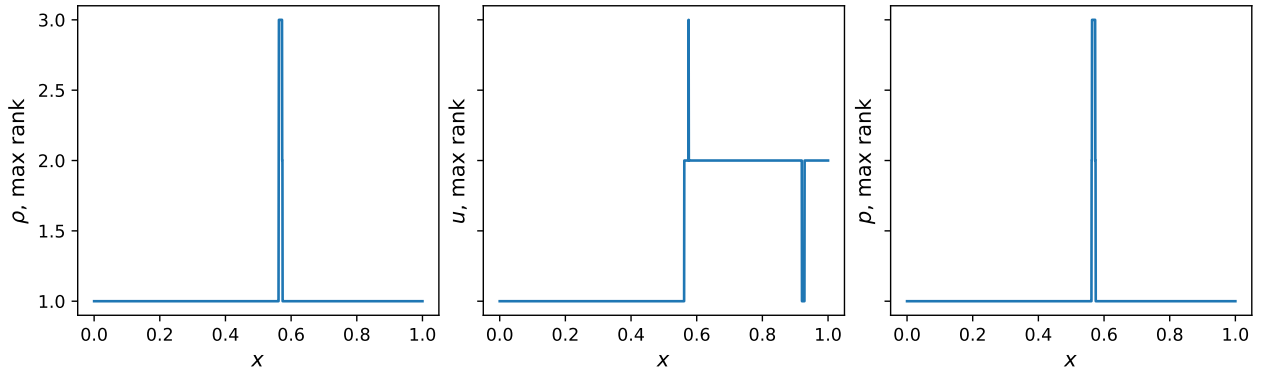


Figure 15: Maximal rank in each spatial cell for ρ, u, p at final time. The results were obtained with $N_x = 1600, N_\xi = 20, r_{\max} = 5, \varepsilon = 0.01$.

the solution at that point. The maximal rank at intermediate times are plotted in Appendix C. As observed in the final time, the high ranks follow the shock. For the velocity, the region to the right of the shock has a larger rank than to the left of the shock. Overall, this test case has the same general behavior as the Sod problem: ranks are kept very low for most spatial cells, and the rank increases near the shock. However, the maximal rank is still small compared to the dimension of the problem and this show the usability of the hybrid format even for more complex test-cases.

6 Conclusion and Outlook

In this paper, we have introduced a new method to use the stochastic finite volume method with many stochastic parameters. The numerical experiments show the feasibility of the approach. A comparison with the full-TT format shows that both methods yield qualitatively similar results. In the current implementation, the full-TT format is more efficient, both in time and number of coefficients. Our current implementation, which uses regular grids and no parallelization, could be easily improved. The hybrid method also has the unique feature that the rank varies in each spatial cell, which allows more adaption to the correlation between the spatial and stochastic variables. It furthermore simply generalizes to arbitrary finite-volume schemes.

This work opens new avenues for combining the tensor train format with an accurate numerical method for hyperbolic equations. Several aspects of the proposed method could be further investigated:

- The choice of appropriate algorithm parameters – such as the TT-rank or the tolerance for TT approximations – is very likely to be problem-dependent. Hence, the algorithm should be tested on other

representative problems and for various probability densities.

- Convergence estimates combining the SFV and the TT approximation are yet to be developed. Our results indicate that the tolerance for the TT approximation has some impact on the convergence rate. Their theoretical estimates is also an ongoing work.
- From the Sod problem and the Shu-Osher problem, it appears that the ranks are generally kept very low, and that larger ranks are required near the shock. The correlation between spatial features and stochastic feature is an interesting topic for future research.

The proposed algorithm is a proof of concept and it may easily be combined with various high-performance computing techniques. The algorithm is easily parallelizable, since the numerical flux is computed independently on each spatial cell. Moreover, the observations from the Sod problem and the Shu-Osher problem indicate a new direction for mesh adaptation methods. The area where the rank increase is also the region where mesh refinement would be the most beneficial: a large rank could be an indicator as to where refinement is needed. For example, the method introduced in [17, 21, 22] for mesh adaptation in physical and stochastic space may be adapted to our setting.

A Algorithms

We describe the method in pseudocode. The general algorithm for the hybrid format is presented in Algorithm 1 and the reconstruction is presented in Algorithm 2. The general algorithm and reconstruction for the full-TT format are presented in Algorithm 3 and Algorithm 4, respectively. The CFL number is denoted by α .

In the full-TT format, the left and right numerical fluxes are computed as follows: the numerical flux at each interface is first computed using the global operations, then the left-shifted flux is computed by applying the matrix \mathbf{L} to the spatial core of the flux. Those operations are described in Algorithm 5.

Every time cross interpolation is used, it is made visible in the pseudocode with the syntax 'cross ($f(T1, T2, \dots)$)'. Here, ' f ' is the non-polynomial function and ' $T1, T2, \dots$ ' are its arguments in the tensor train format.

Remark 1. *In the Algorithms 1 and 3, the maximum of $|f'(\bar{U}^0)|$ can be computed directly in the tensor train format. In tntorch – the tensor train library used for this work – the minimum of a tensor train is computed by minimizing the objective function $x \mapsto \tan(\pi/2 - x)$, where the objective function is evaluated with cross approximation.*

Algorithm 1 MUSCL scheme and forward Euler for the hybrid format

```

for all  $i \in \{1, \dots, N_x N_q\}$  do
     $U_i^0 \leftarrow \text{cross}(u_0(x_i, \xi_1, \dots, \xi_m))$  {Evaluate  $u_0$  for the midpoint rule}
end for
 $\bar{U}^0 \leftarrow \text{Average}(U^0)$ 
 $\Delta t \leftarrow \alpha \frac{\Delta x}{\max |f'(\bar{U}^0)|}$ 
for all  $k \in 0, \dots, N_t$  do
    for all  $i \in \{1, \dots, N_x\}$  do
         $U_{i\pm 1/2}^{n\pm} \leftarrow \text{Reconstruction}(\bar{U}_i^n)$  {Reconstruct values at interfaces, see Algorithm 2 }
         $a \leftarrow \text{cross}(\max(|f'(U_{i+1/2}^+)|, |f'(U_{i+1/2}^-)|))$  {Compute the numerical velocity}
         $H_{i\pm 1/2} \leftarrow \frac{f(U_{i\pm 1/2}^+) + f(U_{i\pm 1/2}^-)}{2\Delta x} - \frac{a(U_{i\pm 1/2}^+ - U_{i\pm 1/2}^-)}{2\Delta x}$  {Compute the left and right fluxes}
         $\bar{U}_i^{n+1} \leftarrow \bar{U}_i^n - \frac{\Delta t}{\Delta x} (H_{i+1/2} - H_{i-1/2})$  {Update the solution}
    end for
end for

```

Algorithm 2 Reconstruction

```
for all  $i \in \{1, \dots, N_x\}$  do
   $(U_x)_i^n \leftarrow \text{cross}(\text{minmod}(U_i - U_{i-1}, U_{i+1} - U_i))$ 
   $U_{i+1/2}^{n+} \leftarrow \bar{U}_{i+1}^n - \frac{1}{2}(U_x)_{i+1}^n$ 
   $U_{i+1/2}^{n-} \leftarrow \bar{U}_i^n + \frac{1}{2}(U_x)_i^n$ 
end for
return  $U_{i+1/2}^{n+}, U_{i+1/2}^{n-}$ 
```

Algorithm 3 MUSCL scheme in the full-TT format

```
 $U^0 \leftarrow \text{cross}(u_0(x_i, \xi_1, \dots, \xi_m))$  {Evaluate  $u_0$  for the midpoint rule}
 $\bar{U}^0 \leftarrow \text{Average}(U^0)$ 
 $\Delta t \leftarrow \alpha \frac{\Delta x}{\max|f'(\bar{U}^0)|}$ 
for all  $k \in 0, \dots, N_t$  do
   $U^{n\pm} \leftarrow \text{ReconstructionFTT}(\bar{U}^n)$  {Reconstruct values at interfaces, see Algorithm 4 }
   $H_L, H_R \leftarrow \text{NumFluxFTT}(U^\pm)$  {Compute the left and right fluxes, see Algorithm 5}
   $\bar{U}^{n+1} \leftarrow \bar{U}_i^n - \frac{\Delta t}{\Delta x}(H_R - H_L)$  {Update the solution}
end for
```

Algorithm 4 Reconstruction in full-TT format

```
 $G_0, G_1, \dots, G_m \leftarrow \text{cores}(\bar{U}^n)$  {Collect the TT-cores of the solution}
 $\tilde{G}_0^L, \tilde{G}_0^R \leftarrow (\mathbf{I} - \mathbf{L})G_0, (\mathbf{R} - \mathbf{I})G_0$ 
 $U_L^n, U_R^n \leftarrow \text{TensorTrain}([\tilde{G}_0^L, G_1, \dots, G_m]), \text{TensorTrain}([\tilde{G}_0^R, G_1, \dots, G_m])$  {Create left- and right-shifted
solution from the modified cores}
 $(U_x)_i^n \leftarrow \text{cross}(\text{minmod}(U_L^n, U_R^n))$ 
 $U^{n\pm} \leftarrow \bar{U}^n \pm \frac{1}{2}(U_x)_i^n$ 
return  $U^{n+}, U^{n-}$ 
```

Algorithm 5 Flux computation in full-TT format

```
 $a \leftarrow \text{cross}(\max(|U^{n+}|, |U^{n-}|))$  {Compute the numerical velocity}
 $H \leftarrow \frac{f(U^{n+}) + U^{n-}}{2} - a \frac{U^{n+} - U^{n-}}{2}$ 
 $G_0, G_1, \dots, G_m \leftarrow \text{cores}(H)$  {Collect the TT-cores of the flux}
 $\tilde{G}_0^L \leftarrow \mathbf{L}G_0$  {Shift the spatial core to one index to the left}
 $H_L \leftarrow \text{TensorTrain}([\tilde{G}_0^L, G_1, \dots, G_m])$  {Create left-shifted flux from the modified cores}
return  $H_L, H$ 
```

B Expectation and variance for the exact solution

We give here the expression for the expectation and variance of the exact solution to the Burgers' equation, for the shock case and for $m \geq 2$.

We assume that $v_m = (v_{L,m} + v_{R,m})/2 \neq 0$ and define

$$\hat{\xi} = (\xi_1, \dots, \xi_{m-1}), \quad \hat{\mathbf{v}}_L = (v_{L,1}, \dots, v_{L,m-1}), \quad (51)$$

$$\hat{\mathbf{v}}_R = (v_{R,1}, \dots, v_{R,m-1}), \quad \hat{\mathbf{v}} = (\hat{\mathbf{v}}_L + \hat{\mathbf{v}}_R)/2. \quad (52)$$

Let $c(t, x, \hat{\xi}) = (x/t - \hat{\mathbf{v}} \cdot \hat{\xi})/v_m$ and

$$a(t, x, \hat{\xi}) = \begin{cases} 1, & c(\hat{\xi}, x, t) > 1, \\ c(t, x, \hat{\xi}), & 0 < c(t, x, \hat{\xi}) < 1, \\ 0, & c(t, x, \hat{\xi}) < 0 \end{cases} = \min(1, \max(0, c(t, x, \hat{\xi}))). \quad (53)$$

The expectation is

$$\begin{aligned} \mathbb{E}[u] &= \int_{[0,1]^{m-1}} \int_{\xi_m=0}^{a(\hat{\xi})} u_R(\hat{\xi}) p_1(\xi_1) \dots p_m(\xi_m) d\xi_m d\hat{\xi} \\ &\quad + \int_{[0,1]^{m-1}} \int_{\xi_m=a(\hat{\xi})}^1 u_L(\hat{\xi}) p_1(\xi_1) \dots p_m(\xi_m) d\xi_m d\hat{\xi}. \end{aligned} \quad (54)$$

For a uniform probability density over $[0, 1]$, that is $p_1 = \dots = p_m = 1$ and using the expression of u_L, u_R and $\mathbf{v}_L, \mathbf{v}_R$,

$$\mathbb{E}[u] = \int_{[0,1]^{m-1}} (-1 + \hat{\mathbf{v}}_R \cdot \hat{\xi}) a + v_{R,m} \frac{a^2}{2} + (1 + \hat{\mathbf{v}}_L \cdot \hat{\xi}) + \frac{v_{L,m}}{2} - (1 + \hat{\mathbf{v}}_L \cdot \hat{\xi}) a - v_{L,m} \frac{a^2}{2} d\hat{\xi}.$$

For the variance we start by computing

$$\begin{aligned} \mathbb{E}[u^2] &= \int_{[0,1]^{m-1}} \left((-1 + \hat{\mathbf{v}}_R \cdot \hat{\xi})^2 a + (-1 + \hat{\mathbf{v}}_R \cdot \hat{\xi}) v_{R,m} a^2 + \frac{v_{R,m}^2}{3} a^3 \right) \\ &\quad - \left((1 + \hat{\mathbf{v}}_L \cdot \hat{\xi})^2 a + (1 + \hat{\mathbf{v}}_L \cdot \hat{\xi}) v_{L,m} a^2 + \frac{v_{L,m}^2}{3} a^3 \right) \\ &\quad + \left((1 + \hat{\mathbf{v}}_L \cdot \hat{\xi})^2 + (1 + \hat{\mathbf{v}}_L \cdot \hat{\xi}) v_{L,m} + \frac{v_{L,m}^2}{3} \right) d\hat{\xi}. \end{aligned} \quad (55)$$

The variance is then obtained with $\text{Var}[u(t, x)] = \mathbb{E}[u(t, x)^2] - \mathbb{E}[u(t, x)]^2$.

C Shu-Osher problem: maximal ranks at various timesteps

Figures 16–19 show the maximal rank in each spatial cell for the solution ρ, u, p of the Shu-Osher problem at times $t \in \{0.0, 0.04, 0.07, 0.1\}$. The results were obtained with $N_x = 1600$, $N_\xi = 20$, $r_{\max} = 5$ and $\varepsilon = 0.01$.

Acknowledgments

We would like to thank Adrian Kolb for providing the Monte-Carlo results, and the anonymous reviewer for his useful comments.

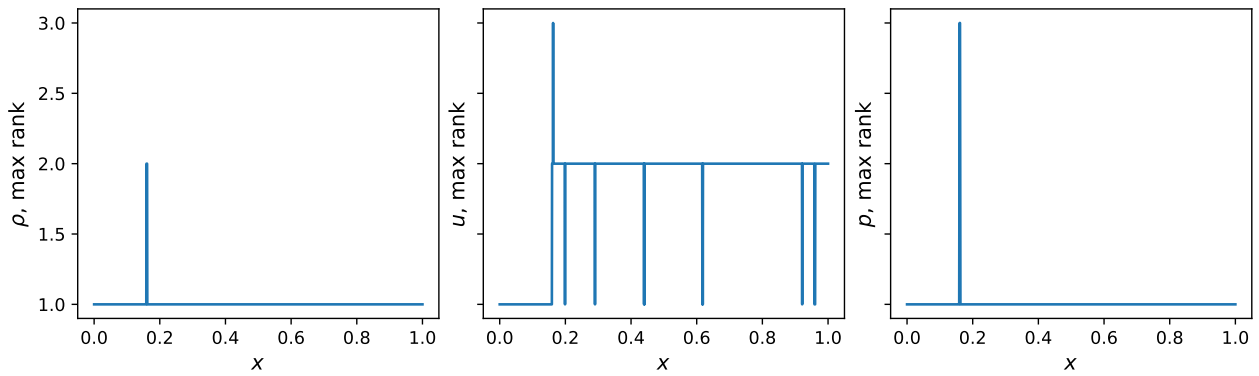


Figure 16: Maximal rank in each spatial cell for ρ, u, p at initial time.

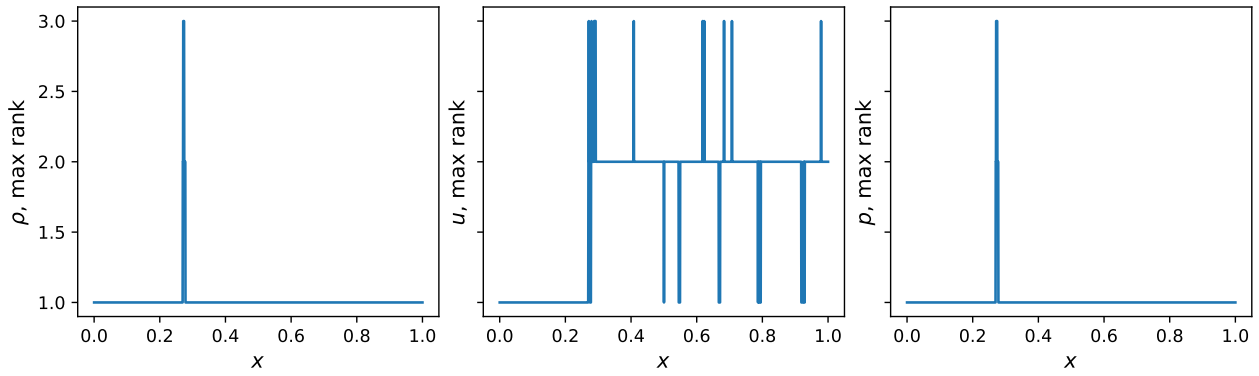


Figure 17: Maximal rank in each spatial cell for ρ, u, p at time $t = 0.04$.

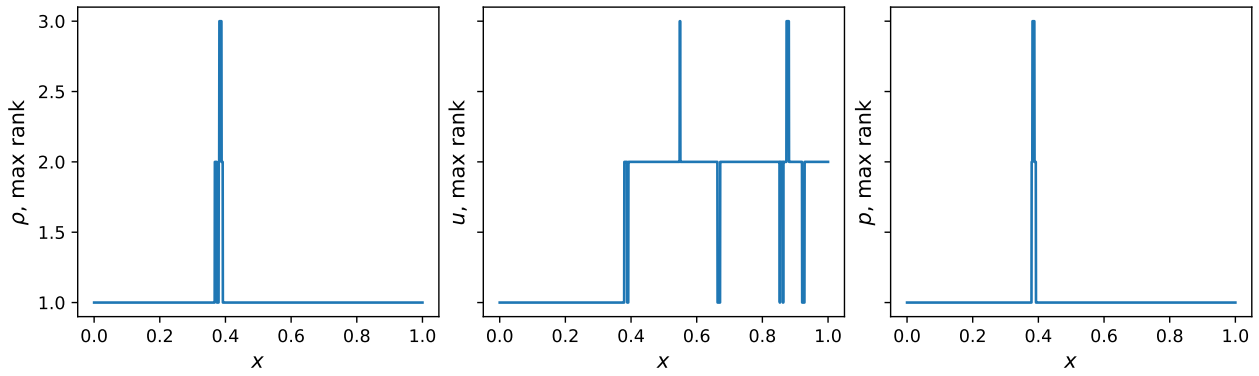


Figure 18: Maximal rank in each spatial cell for ρ, u, p at time $t = 0.07$.

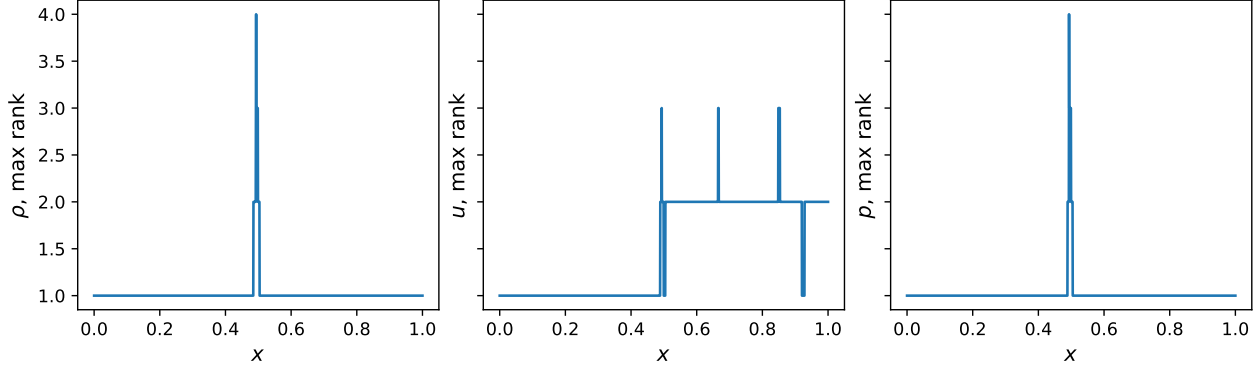


Figure 19: Maximal rank in each spatial cell for ρ, u, p at time $t = 0.1$.

References

- [1] T. Barth. "On the propagation of statistical model parameter uncertainty in CFD calculations". In: *Theoretical and Computational Fluid Dynamics* 26.5 (Oct. 2012), pp. 435–457. ISSN: 0935-4964, 1432-2250. DOI: 10.1007/s00162-011-0221-2. URL: <http://link.springer.com/10.1007/s00162-011-0221-2>.
- [2] S. Mishra and C. Schwab. "Sparse tensor multi-level Monte Carlo finite volume methods for hyperbolic conservation laws with random initial data". In: *Mathematics of Computation* 81.280 (Apr. 5, 2012), pp. 1979–2018. ISSN: 0025-5718, 1088-6842. DOI: 10.1090/S0025-5718-2012-02574-9. URL: <https://www.ams.org/mcom/2012-81-280/S0025-5718-2012-02574-9/>.
- [3] M. Bachmayr. "Low-rank tensor methods for partial differential equations". In: *Acta Numerica* 32 (May 2023), pp. 1–121. ISSN: 0962-4929, 1474-0508. DOI: 10.1017/S0962492922000125. URL: https://www.cambridge.org/core/product/identifier/S0962492922000125/type/journal_article.
- [4] I. Oseledets. "Tensor-Train Decomposition". In: *SIAM Journal on Scientific Computing* 33.5 (Jan. 2011), pp. 2295–2317. ISSN: 1064-8275, 1095-7197. DOI: 10.1137/090752286. URL: <http://pubs.siam.org/doi/10.1137/090752286>.
- [5] E. Kornev, S. Dolgov, K. Pinto, M. Pflitsch, M. Perelshtain, and A. Melnikov. *Numerical solution of the incompressible Navier-Stokes equations for chemical mixers via quantum-inspired Tensor Train Finite Element Method*. <http://arxiv.org/abs/2305.10784>. May 23, 2023. arXiv: 2305.10784 [physics, physics:quant-ph]. URL: <http://arxiv.org/abs/2305.10784>.
- [6] Z. Zhong, S. Wang, and K. Wang. "Fast Low-Rank Solution of the Multidimensional Hyperbolic Problems". In: *Computational Mathematics and Modeling* 29.3 (July 2018), pp. 344–358. ISSN: 1046-283X, 1573-837X. DOI: 10.1007/s10598-018-9414-5. URL: <http://link.springer.com/10.1007/s10598-018-9414-5>.
- [7] S. Walton, S. Tokareva, and G. Manzini. *The Tensor-Train Stochastic Finite Volume Method for Uncertainty Quantification*. <https://arxiv.org/abs/2404.06574>. 2024. arXiv: 2404.06574 [math.NA]. URL: <https://arxiv.org/abs/2404.06574>.
- [8] R. Abgrall and S. Tokareva. "The Stochastic Finite Volume Method". In: *Uncertainty Quantification for Hyperbolic and Kinetic Equations*. Ed. by S. Jin and L. Pareschi. Vol. 14. Springer International Publishing, 2017, pp. 1–57. ISBN: 978-3-319-67109-3 978-3-319-67110-9. DOI: 10.1007/978-3-319-67110-9_1. URL: http://link.springer.com/10.1007/978-3-319-67110-9_1.
- [9] A. Kurganov and E. Tadmor. "New High-Resolution Central Schemes for Nonlinear Conservation Laws and Convection–Diffusion Equations". In: *Journal of Computational Physics* 160.1 (May 2000), pp. 241–282. ISSN: 00219991. DOI: 10.1006/jcph.2000.6459. URL: <https://linkinghub.elsevier.com/retrieve/pii/S0021999100964593>.

[10] V. De Silva and L.-H. Lim. "Tensor Rank and the Ill-Posedness of the Best Low-Rank Approximation Problem". In: *SIAM Journal on Matrix Analysis and Applications* 30.3 (Jan. 2008), pp. 1084–1127. ISSN: 0895-4798, 1095-7162. DOI: 10.1137/06066518X. URL: <http://pubs.siam.org/doi/10.1137/06066518X>.

[11] I. Oseledets and E. Tyrtyshnikov. "TT-cross approximation for multidimensional arrays". In: *Linear Algebra and its Applications* 432.1 (Jan. 2010), pp. 70–88. ISSN: 00243795. DOI: 10.1016/j.laa.2009.07.024. URL: <https://linkinghub.elsevier.com/retrieve/pii/S0024379509003747> (visited on 01/13/2025).

[12] D. Savostyanov and I. Oseledets. "Fast adaptive interpolation of multi-dimensional arrays in tensor train format". In: *The 2011 International Workshop on Multidimensional (nD) Systems*. 2011 7th International Workshop on Multidimensional (nD) Systems (nDS 2011). Poitiers, France: IEEE, Sept. 2011, pp. 1–8. ISBN: 978-1-61284-815-0. DOI: 10.1109/nDS.2011.6076873. URL: <http://ieeexplore.ieee.org/document/6076873/>.

[13] D. V. Savostyanov. "Quasioptimality of maximum-volume cross interpolation of tensors". In: *Linear Algebra and its Applications* 458 (Oct. 2014). Publisher: Elsevier BV, pp. 217–244. ISSN: 0024-3795. DOI: 10.1016/j.laa.2014.06.006. URL: <https://linkinghub.elsevier.com/retrieve/pii/S0024379514003711> (visited on 01/14/2025).

[14] A. I. Osinsky. "Tensor Trains Approximation Estimates in the Chebyshev Norm". In: *Computational Mathematics and Mathematical Physics* 59.2 (Feb. 2019). Publisher: Pleiades Publishing Ltd, pp. 201–206. ISSN: 0965-5425, 1555-6662. DOI: 10.1134/s096554251902012x. URL: <http://link.springer.com/10.1134/S096554251902012X>.

[15] Z. Qin, A. Lidiak, Z. Gong, G. Tang, M. B. Wakin, and Z. Zhu. "Error Analysis of Tensor-Train Cross Approximation". In: *Proceedings of the 36th International Conference on Neural Information Processing Systems*. Curran Associates Inc., 2022. ISBN: 978-1-7138-7108-8. DOI: 10.5555/3600270.3601305.

[16] M. Herty, A. Kolb, and S. Müller. "Higher-Dimensional Deterministic Approach for Conservation Laws with Random Initial Data". In: *Hyperbolic Problems: Theory, Numerics, Applications. Volume II*. Ed. by C. Parés, M. J. Castro, T. Morales De Luna, and M. L. Muñoz-Ruiz. Vol. 35. Springer Nature Switzerland, 2024, pp. 111–120. ISBN: 978-3-031-55263-2 978-3-031-55264-9. DOI: 10.1007/978-3-031-55264-9_10. URL: https://link.springer.com/10.1007/978-3-031-55264-9_10.

[17] A. J. Kolb. "Multiresolution-based grid adaptation for hyperbolic conservation laws with uncertain initial data". Veröffentlicht auf dem Publikationsserver der RWTH Aachen University 2024; Dissertation, RWTH Aachen University, 2023. Dissertation. Aachen: RWTH Aachen University, 2023, 1 Online–Ressource : Illustrationen. DOI: 10.18154/RWTH-2024-00677. URL: <https://publications.rwth-aachen.de/record/977250>.

[18] M. Usyatsov, R. Ballester-Ripoll, and K. Schindler. "tntorch: Tensor Network Learning with PyTorch". In: *Journal of Machine Learning Research* 23.208 (2022), pp. 1–6. ISSN: 1533-7928. URL: <http://jmlr.org/papers/v23/21-1197.html>.

[19] P. Virtanen et al. "SciPy 1.0: fundamental algorithms for scientific computing in Python". In: *Nature Methods* 17.3 (Mar. 2, 2020), pp. 261–272. ISSN: 1548-7091, 1548-7105. DOI: 10.1038/s41592-019-0686-2. URL: <https://www.nature.com/articles/s41592-019-0686-2>.

[20] N. Gerhard, F. Iacono, G. May, S. Müller, and R. Schäfer. "A High-Order Discontinuous Galerkin Discretization with Multiwavelet-Based Grid Adaptation for Compressible Flows". In: *Journal of Scientific Computing* 62 (2015), pp. 25–52. ISSN: 1573-7691. DOI: 10.1007/s10915-014-9846-9. URL: <https://doi.org/10.1007/s10915-014-9846-9>.

[21] M. Herty, A. Kolb, and S. Müller. "Multiresolution analysis for stochastic hyperbolic conservation laws". In: *IMA Journal of Numerical Analysis* 44.1 (Feb. 2, 2024), pp. 536–575. ISSN: 0272-4979, 1464-3642. DOI: 10.1093/imanum/drad010. URL: <https://academic.oup.com/imajna/article/44/1/536/7080301>.

[22] M. Herty, A. Kolb, and S. Müller. "A novel multilevel approach for the efficient computation of random hyperbolic conservation laws". In: *Multiscale, Nonlinear and Adaptive Approximation II*. Ed. by R. DeVore and A. Kunoth. Cham: Springer Nature Switzerland, 2024, pp. 327–346. ISBN: 978-3-031-75802-7. DOI: 10.1007/978-3-031-75802-7_15. URL: https://doi.org/10.1007/978-3-031-75802-7_15.